Applied Catalysis B: Environmental 150–151 (2014) 596–604

Contents lists available at ScienceDirect

Applied Catalysis B: Environmental

journal homepage: www.elsevier.com/locate/apcatb

# Butadiene production from bioethanol and acetaldehyde over tantalum oxide-supported ordered mesoporous silica catalysts

Ho-Jeong Chae*, Tae-Wan Kim**, Young-Kyun Moon, Han-Kyu Kim, Kwang-Eun Jeong, Chul-Ung Kim, Soon-Yong Jeong***

*Green Chemistry Research Division, Korea Research Institute of Chemical Technology, P.O. Box 107, 141 Gajeong-ro, Yuseong-gu, Daejeon 305-600, Republic of Korea*

ARTICLE INFO

*Article history:*
Received 2 June 2013
Received in revised form
10 December 2013
Accepted 14 December 2013
Available online 24 December 2013

*Keywords:*
Ethanol to butadiene
Ordered mesoporous silica
Tantalum oxide
Pore structure

ABSTRACT

A series of ordered mesoporous silica (OMS) supported tantalum oxide samples (Ta/OMS) were tested as catalysts for the production of 1,3-butadiene (BD) from ethanol and acetaldehyde. To study the influence of the type of mesostructure, the pore size, and the particle morphology on the performance of the catalyst, Ta/OMS catalysts were prepared using two different mesostructured silica supports (2-D hexagonal SBA-15 and 3-D cubic KIT-6) and five different 2-D hexagonal OMS supports (SBA-15 series and MMS) with varied mesopore diameters in the range of 2.5–10.9 nm. The obtained Ta/OMS catalysts were characterized by a nitrogen physisorption analysis and X-ray diffraction, as well as by scanning electron micrography. The catalytic results showed that the pore size and crystal size of OMS samples are more important than mesopore structure such as pore dimension and pore shape to optimize the catalytic performance of Ta/OMS catalysts for BD production from ethanol and acetaldehyde.



## 1. Introduction

1,3-Butadiene (BD) is an important chemical intermediate material in the petroleum chemical industry. BD is generally used as a starting material for commercially important synthetic rubbers and polymers such as styrene–butadiene rubber, polybutadiene, styrene–butadiene latex, acrylonitrile–butadiene–styrene polymer and nitrile rubber [1]. Recently, BD has received more attention due to the rapid economic growth of developing countries such as China and India.

Nowadays, the dominant technology for the production of BD is the naphtha cracking process, where BD is obtained as a co-product. However, the increasing rate of BD demand may lead to a serious shortage in BD production by current naphtha cracking processes. Moreover, in order to cope with the depletion of petroleum reserves, high oil prices and environmental issues including global warming, it is crucial to develop alternative technologies for BD production from renewable, non-petroleum resources such as bioethanol. Bioethanol is one of the most abundant sustainable raw materials of "bio-carbon" sources today [1,2]. Therefore, in the near future, BD production using bioethanol will be the most promising, sustainable and renewable technology among various on-purpose BD production technologies.

The catalytic conversion of ethanol into BD (ETB) is an old industrially proven process which was used from the 1920s to the early 1960s. This process was completely scrapped with increasing oil production after the development of large oilfields. However, the ETB process is becoming more attractive recently as a potential alternative route due to the high oil prices and wide supply of bioethanol. ETB processes are divided into a one-step process developed by Sergey Lebedev using a variety of mixed metal oxide catalysts [1–9] and a two-step process which is also known as Ostromyslensky's process and which was commercialized by Carbide and Carbon Chemicals Corporation in the USA using tantalum oxide silica as a second-step catalyst [10–15]. The two-step process includes partial ethanol dehydrogenation to acetaldehyde as the first step, followed by the transformation of the mixture of ethanol and acetaldehyde into BD as the second step. Both processes have short catalyst regeneration cycles, which are 12 h for one-step process and 120 h for two-step process [10–15], due to rapid catalyst deactivation by coking. This short regeneration cycle should be upgraded by developing catalysts tolerable to coke because it is main cause lowering the efficiency of both ETB processes. Few catalyst studies [16,17] of the two-step ETB process has been reported after several papers [10–15] published in the 1940s. In the previous literatures, several metal oxides including tantalum oxide had been screened simply for a comparison of their activity levels and

* Corresponding author. Tel.: +82 42 860 7290; fax: +82 42 860 7508.
** Corresponding author. Tel.: +82 42 860 7257; fax: +82 42 860 7508.
*** Corresponding author. Tel.: +82 42 860 7538; fax: +82 42 860 7508.
*E-mail addresses:* hjchae@krict.re.kr (H.-J. Chae), twkim@krict.re.kr (T.-W. Kim), syjeong@krict.re.kr (S.-Y. Jeong).

0926-3373/$ – see front matter © 2014 Elsevier B.V. All rights reserved.
http://dx.doi.org/10.1016/j.apcatb.2013.12.023

BD selectivity characteristics. Especially, in tantala–silica catalyst system, no study for the influence of the type and properties of silica, which plays a role in support as well as catalyst in two-step ETB reaction, has reported although the type and physicochemical properties of the silica is very important factor for the optimization of the catalyst durability as well as the activity and selectivity in BD production.

The mechanism of the ethanol or ethanol/acetaldehyde to BD is very complicated and is still debating [1,2]. However, several literatures [1,2,9] had reported the following five principal steps: (1) acetaldehyde formation from ethanol; (2) aldol condensation of acetaldehyde to acetaldol; (3) dehydration of acetaldol to crotonaldehyde; (4) Meerwein–Ponndorf–Verley reaction between crotonaldehyde and ethanol to obtain crotyl alcohol and acetaldehyde; and (5) dehydration of crotyl alcohol to BD. Based upon the reaction mechanism, the ETB catalysts should have not only the redox ability but also the proper acidic and basic properties. Thus, the roles of supports as well as active metal oxides are very important.

In this study, a variety of ordered mesoporous silica (OMS) samples were synthesized and examined as a potential new support for a tantalum oxide base catalyst to be used in the two-step process. Moreover, the effect of the physical structure and properties of OMS on the performance of the two-step ETB reaction was examined and optimized by comparing OMS supports with different pore structures, pore sizes and crystal sizes. In this case, we used SBA-15 series, KIT-6 and MMS. This is the first study to apply various OMSs as a support and examine the effect of the pore size, pore structure and morphology of the OMSs on an ETB reaction.

## 2. Experimental

### 2.1. Synthesis of ordered mesoporous silica (OMS) supports

The ordered mesoporous silica support SBA-15 with a 2-D hexagonal structure was prepared by the procedure reported by Choi et al. [18]. 33.6 g of triblock copolymer Pluronic P123 ($EO_{20}PO_{70}EO_{20}$, Aldrich) was fully dissolved in 18.3 g of 0.3 M HCl aqueous solution at 35 °C. After the addition of 54.2 g of tetraethyl orthosilicate (TEOS, Aldrich) to the solution, the mixture was stirred for 1 day and the reaction mixture was hydrothermally treated in a Teflon-lined autoclave at 35–130 °C for 1 day. After the hydrothermal treatment, the resulting white solid product was filtrated and dried at 100 °C in air. Finally, an organic template-free SBA-15 mesoporous silica support was obtained by a calcination process at 550 °C, and the SBA-15 OMS supports were designated as SBA-15-*T*, where *T* represents the hydrothermal treatment temperature of the SBA-15 OMS support.

Ordered mesoporous silica KIT-6 material with a 3-D cubic *Ia–3d* structure was prepared following the process reported by Kim [19]. Briefly, 16.9 g of Pluronic P123 and 18.6 g of *n*-butanol (Aldrich) were dissolved in an aqueous HCl solution (33.2 g of HCl in 610.1 g of water). After complete dissolution, 43.6 g of TEOS was added to the mixture solution at 35 °C. After magnetic stirring for 1 day at 35 °C, the mixture was aged at 100 °C for 1 day in an oven as a hydrothermal treatment. After the hydrothermal treatment, the solid product was recovered by filtration and dried. The final KIT-6 support was obtained by calcination at 550 °C.

MCM-41-type ordered mesoporous silica MMS support was synthesized using a fluorosilicon compound as a silica source according to a procedure described earlier [20]. A hydrofluosilicic acid solution ($H_2SiF_6$) was prepared by gradually dissolving 10 g of fumed silica in 32.5 g of 24 wt% HF (Merck) and 25 ml of water. The $H_2SiF_6$ solution was added to 30.6 g of cetyltrimethyl ammonium bromide (CTMABr, Aldrich) in 600 g of distilled water and stirred at 60 °C for 1 h. A white gel was formed upon the addition of 150 g of 28Ywt% $NH_4OH$ solution, and this was vigorous stirred at the same temperature for 1 h. The mixture was moved to an oven and aged at 70 °C for 16 h. After filtration, the solid was washed with water and dried at 100 °C. The dried sample was calcined at 600 °C for 4 h to remove the surfactant.

### 2.2. Preparation of catalysts

All of the ordered mesoporous silica-supported 2Ywt% tantalum oxide ($Ta_2O_5$) catalysts were prepared by an impregnation method using ethanol as a solvent. 1 g of OMS support was added to 100 ml of ethanol which contained 0.32 g of tantalum pentachloride ($TaCl_5$, Aldrich). After stirring for 2 h, the ethanol was removed by a rotary evaporator and the samples were dried at 120 °C for 10 h. The OMS-supported $Ta_2O_5$ samples (Ta/OMS) were obtained by calcination at 500 °C for 5 h. For comparison, two different commercial silica gels, Grade 62 and Silica gel 60, were obtained by Aldrich and Merck, respectively, and two different $Ta_2O_5$-supported commercial silica gels were obtained by the same impregnation method. These are denoted as Ta/Aldrich and Ta/Merck, respectively.

### 2.3. Characterization

Powder X-ray diffraction (XRD) patterns were recorded on a Rigaku Multiplex instrument using Cu-Kα radiation ($\lambda_Y$= 0.15406 nm) operated at 40 kV and 40 mA (1.6 kW). Nitrogen adsorption isotherms were measured at −196 °C on a Micromeritics Tristar 3000 volumetric adsorption analyzer. Before the adsorption measurements, all samples were outgassed at 300 °C in a degassing station. The Brunauer–Emmett–Teller (BET) equation was used to calculate the apparent surface area from the adsorption data obtained at $P/P_0$ between 0.05 and 0.2. The total volume of micro- and mesopores was calculated from the amount of nitrogen adsorbed at $P/P_0$ = 0.95, assuming that adsorption on the external surface was negligible compared to adsorption in the pores. The pore size distributions (PSDs) were calculated by analyzing the adsorption branch of the $N_2$ sorption isotherm using the Barret–Joyner–Halenda (BJH) method. The external surface ($S_{ext}$) area was estimated from the nitrogen adsorption data using the $\alpha_s$-plot method [21,22] in the $\alpha_s$ range of 1.7–2.7 (exceptionally, 2.2–6.6 for Aldrich and Ta/Aldrich samples). The reference adsorption isotherm reported elsewhere [23] used in these calculations.

Scanning electron micrograph (SEM) images were obtained with a Philips XL-30S FEG scanning electron microscope operated at 10 kV. The samples were coated with gold before the SEM measurement. Transmission electron microscopy (TEM) images were taken from the thin edges of the particles supported on a porous carbon grid, using a Philips Tecnai G220 device operated at 200 kV. Scanning transmission electron microscopy (STEM)/energy-dispersive X-ray spectroscopy (EDS) elemental mapping images were taken with a Tecnai G2 F30 instrument with an accelerating voltage of 300 kV. Coke depositions of catalyst were investigated by recording weight changes on a thermogravimetric analyzer (TA Instruments TGA Q500). Runs under air were carried out with a heating rate of 10.0 °C/min from 100 °C to 700 °C after preheating at 100 °C for 1 h to remove water, reactants and products adsorbed weakly. CHN elemental analysis was carried out by using a Fisons EA 1108 instrument for the determination of the amount of carbon on the catalyst after the reaction.

### 2.4. Catalytic test

The production of 1,3-butadiene (BD) from ethanol and acetaldehyde was performed in a fixed bed reactor system with a 3/8Yin. stainless steel (SUS) tube reactor, as shown in Fig. 1. The

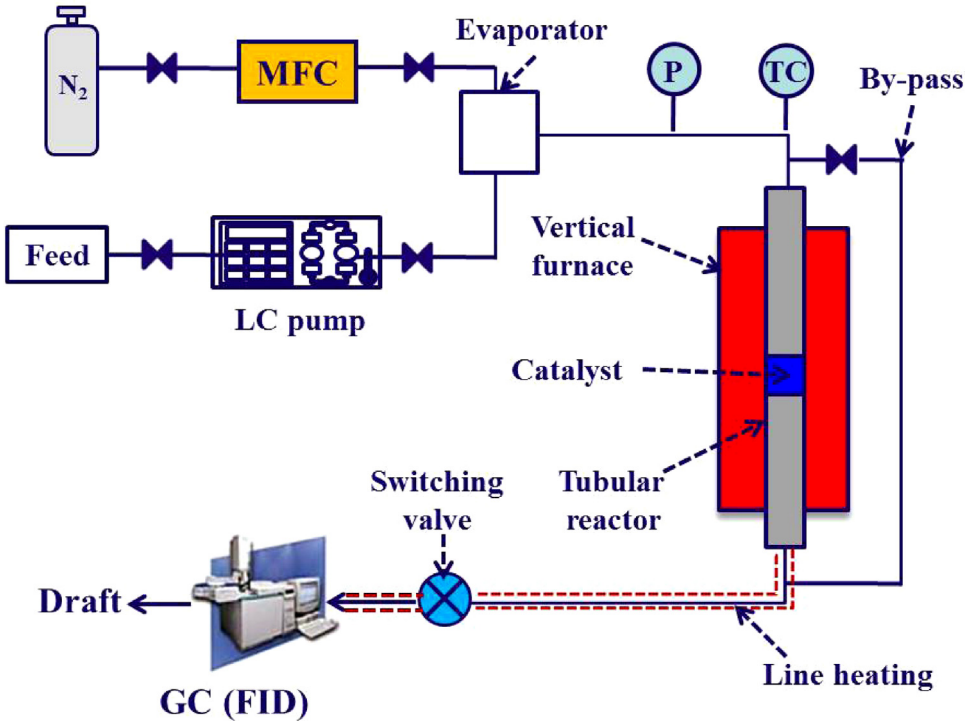


**Fig. 1.** Reaction apparatus for 1,3-butadiene production from ethanol and acetaldehyde.

reaction temperature was controlled by a type-K thermocouple (Omega) and a PID controller. A mixture of ethanol (99.9%wt%, Samchun) and acetaldehyde (85%wt%, Aldrich) with ethanol to acetaldehyde molar ratio of 2.5, which is selected as an optimal ratio confirmed by our preliminary test and the previous literatures [10,14], was fed into the catalytic reactor at 0.66 ml/h by a high-performance liquid chromatography (HPLC) pump. The catalyst (0.25 g) was loaded in the middle of the SUS tube. Before the reaction, the catalyst was warmed up to the reaction temperature (350 °C, heating rate = 5.0 °C/min) with an $N_2$ flow (5 ml/min) as the carrier gas. The reaction was then performed with a liquid hourly space velocity (LHSV) of 1.0 $h^{-1}$ at 350 °C. Catalyst regeneration was carried out with air of 10 ml/min at 500 °C for 5 h. The effluent gas products were measured by a gas chromatograph (6100GC, Young Lin Instrument Co.) equipped with a flame ionization detector (FID). Products were detected by the FID using a capillary HP Plot Q column (0.53 mm id × 40 μm thickness × 30 m length).

In this study, total conversions and BD selectivities were calculated by the following equations.

$$\text{Total conversion} = \frac{(\text{Total C moles} - (\text{C mole}_{\text{unreacted EtOH}} + \text{C mole}_{\text{unreacted AA}}))}{\text{Total C moles}} \times 100$$

$$\text{BD selectivity} = \frac{\text{C mole}_{\text{BD in products}}}{\text{Total C moles in products except for EtOH and AA}} \times 100$$

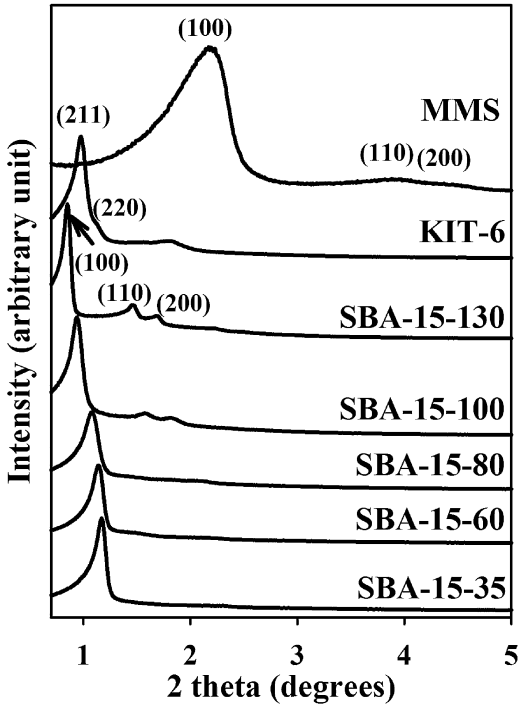


**Fig. 2.** Low angle XRD patterns of 2 wt% $Ta_2O_5$ supported MMS, KIT-6, and SBA-15 OMS catalysts with different hydrothermal temperatures.

## 3. Results and discussion

### 3.1. Properties of OMS supported $Ta_2O_5$ catalysts (Ta/OMSs)

Fig. 2 shows low-angle XRD patterns of the ordered mesoporous silica supported 2%wt% tantalum oxide catalysts. The Ta/SBA-15 catalysts prepared at various temperatures exhibit XRD diffraction patterns characteristic of a 2-D hexagonal mesostructure. Three distinct XRD peaks are shown. These can be indexed as (1 0 0), (1 1 0) and (2 0 0). With an increase in the hydrothermal treatment

**Table 1**
Structural properties of supports and catalysts.

| Samples | $a$ (nm) | $S_{BET}$ ($m^2\ g^{-1}$) | $S_{ext}$ ($m^2\ g^{-1}$) | $V_t$ ($cm^3\ g^{-1}$) | $w_{BJH}$ (nm) |
|---|---|---|---|---|---|
| SBA-15-60 | 9.0 | 710 | 20 | 0.48 | 4.6 |
| SBA-15-80 | 9.4 | 775 | 30 | 0.57 | 5.3 |
| SBA-15-100 | 10.8 | 805 | 50 | 0.93 | 8.0 |
| SBA-15-130 | 12.0 | 583 | 20 | 1.48 | 10.9 |
| KIT-6 | 22.3 | 795 | 20 | 0.92 | 7.9 |
| MMS | 4.7 | 800 | 100 | 0.69 | 2.5 |
| Aldrich | – | 275 | 10 | 1.14 | 13.4[a] |
| Merck | – | 460 | 30 | 0.77 | 5.5[a] |
| Ta/SBA-15-60 | 9.0 | 700 | 20 | 0.47 | 4.6 |
| Ta/SBA-15-80 | 9.4 | 770 | 30 | 0.56 | 5.3 |
| Ta/SBA-15-100 | 10.8 | 800 | 50 | 0.93 | 8.0 |
| Ta/SBA-15-130 | 12.0 | 580 | 20 | 1.48 | 10.9 |
| Ta/KIT-6 | 22.3 | 790 | 20 | 0.91 | 7.9 |
| Ta/MMS | 4.7 | 790 | 100 | 0.68 | 2.5 |
| Ta/Aldrich | – | 270 | 10 | 1.14 | 13.4[a] |
| Ta/Merck | – | 450 | 30 | 0.77 | 5.5[a] |

$a$, XRD unit-cell parameters for the 2-D hexagonal lattice (SBA-15, MMS) and 3-D cubic lattice (KIT-6) equal $6^{1/2}d_{100}$ and $6^{1/2}d_{211}$, respectively; $S_{BET}$, apparent BET specific surface area; $S_{ext}$, external surface area estimated by $\alpha_s$-plot; $V_t$, total pore volume; $w_{BJH}$, the pore size calculated using the BJH method and deduced from the highest point of pore size distribution curve.

[a] BJH average pore diameter.

temperature of the SBA-15 OMS support, the *d*-spacing and lattice parameter gradually increased, which indicates an increase in the mesopore size. Among these Ta/SBA-15 samples, there are some pronounced differences in the relative peak sharpness and distinction. The overall XRD peaks of the Ta/SBA-15 sample with the high hydrothermal temperature, denoted here as Ta/SBA-15-100 and Ta/SBA-15-130, are sharper and more distinct than those of Ta/SBA-15 prepared at a low temperature, indicating that a high degree of mesoscopic ordering resulted from the hydrothermal treatment at a high temperature.

As shown in Fig. 3(a), the nitrogen physisorption isotherms for the four different Ta/SBA-15 samples show a type IV isotherm with a capillary condensation step. The capillary condensation step is sharpened and increased with an increase in the hydrothermal temperature. In addition, the capillary condensation step is gradually shifted to a higher relative pressure with an increasing temperature, indicating that the size of the mesopores of the SBA-15 support can be enlarged by a hydrothermal treatment at a high temperature. The pore size distribution curves for the Ta/SBA-15 samples shown in Fig. 3(a) also clearly show an increase in the mesopore size after increasing the hydrothermal temperature. The structural properties of the Ta/SBA-15 samples prepared at various temperatures are summarized in Table 1. The pore sizes of the Ta/SBA-15 catalysts are shown to range from 4.6 to 10.9 nm with different hydrothermal temperatures, while the pore volumes are significantly increased from 0.47 to 1.48 $cm^3/g$ with an increase in the temperature, which is mostly caused by the increase in the mesopore volume of the SBA-15 support.

The XRD diffraction patterns of the Ta/MMS sample in Fig. 2 are similar to those of Ta/SBA-15 sample, while the first diffraction peak of Ta/MMS appears at higher 2 theta angles (2 theta > 2.0°). This occurs because the MCM-41-type MMS material has the same 2-D hexagonal pore structure as the SBA-15 OMS material, but with a relatively small pore size compared to that of SBA-15. Fig. 3(b) shows the nitrogen isotherm and pore size distribution curve of the Ta/MMS catalyst. The isotherm of Ta/MMS exhibits the appearance of a typical type IV isotherm of a mesoporous material with a capillary condensation step around $P/P_0 = 0.3$; the BET-specific surface area is similar to that of Ta/SBA-15-100 and Ta/KIT-6. However, the pore size distribution curve shows the smallest mesopore (2.5 nm) size among all catalysts.

The other ordered mesoporous material, KIT-6, was prepared by the same structure-directing agent (Pluronic P123) and a synthesis procedure similar to that of SBA-15 material. However, the addition of *n*-butanol (BuOH) leads to the formation of the cubic *Ia*–3*d* phase because BuOH plays a role of a co-structure-directing agent and a co-solvent [19]. Fig. 2 shows the XRD pattern of KIT-6, indicating good structural order with the body-centered cubic *Ia*–3*d* space group. As depicted in Fig. 3(b), the nitrogen sorption isotherm of the Ta/KIT-6 catalyst is a typical type IV isotherm with a noticeable capillary condensation step, which reveals the high ordering of the mesopore structure. The BET-specific surface area, total pore volume, and pore size of the Ta/KIT-6 sample are similar to those of the Ta/SBA-15-100 sample due to the same hydrothermal treatment temperature and Pluronic P123 as the soft structure-directing agent.

SEM images of tantalum-oxide-loaded ordered mesoporous silica supports are displayed in Fig. 4. Fig. 4(a) shows a SEM image of Ta/SBA-15-100, showing a typical hexagonal rod-like SBA-15 morphology with a primary particle size of around 2–4 μm. However, the Ta/KIT-6 and Ta/MMS samples show randomly amorphous particles and small sphere-like primary particles with particle diameters of around 50–120 nm, respectively. The representative TEM images for each Ta/OMS catalysts are shown in Fig. 5. The TEM images confirmed the highly ordered pore-arrangement of the OMS supported Ta catalysts.

Ta/silica catalysts were analyzed by the wide angle X-ray diffraction pattern for the verification of the loading of tantalum oxide and estimation of the particle size of tantalum oxide on the silica supports. But the wide-angle XRD patterns of all silica-supported tantalum oxide catalysts below 20 wt% Ta-oxide loading showed no characteristic peak of the tantalum oxide phase (data not shown), which indicates high dispersion of the Ta species, and it is difficult to estimate the particle size of tantalum oxide using the Scherrer's equation with XRD pattern in the case of the low loading of Ta on silica support [24].

The SBA-15-100 supported 2 wt% Ta catalyst was examined by energy-dispersive X-ray spectroscopy (EDS) elemental mapping analysis conducted in scanning transmission electron microscopy (STEM) as a representative sample. As shown in Fig. 6, STEM/EDS elemental maps of Ta/SBA-15-100 sample clearly show the presence of Ta in the silica support. The X-ray emission from the Si-Kα shell exhibits the Si-Kα signal map in Fig. 6(b), which is the same location of the STEM image in Fig. 6(a). In addition, the X-ray peak count maps of Ta-M (Fig. 6(c)) and Ta-Lα (Fig. 6(d)) appear to be the same location of the STEM image and Si-Kα map. These STEM/EDS maps should indicate that Ta species are existed in the whole silica support with high dispersion, which accords well with

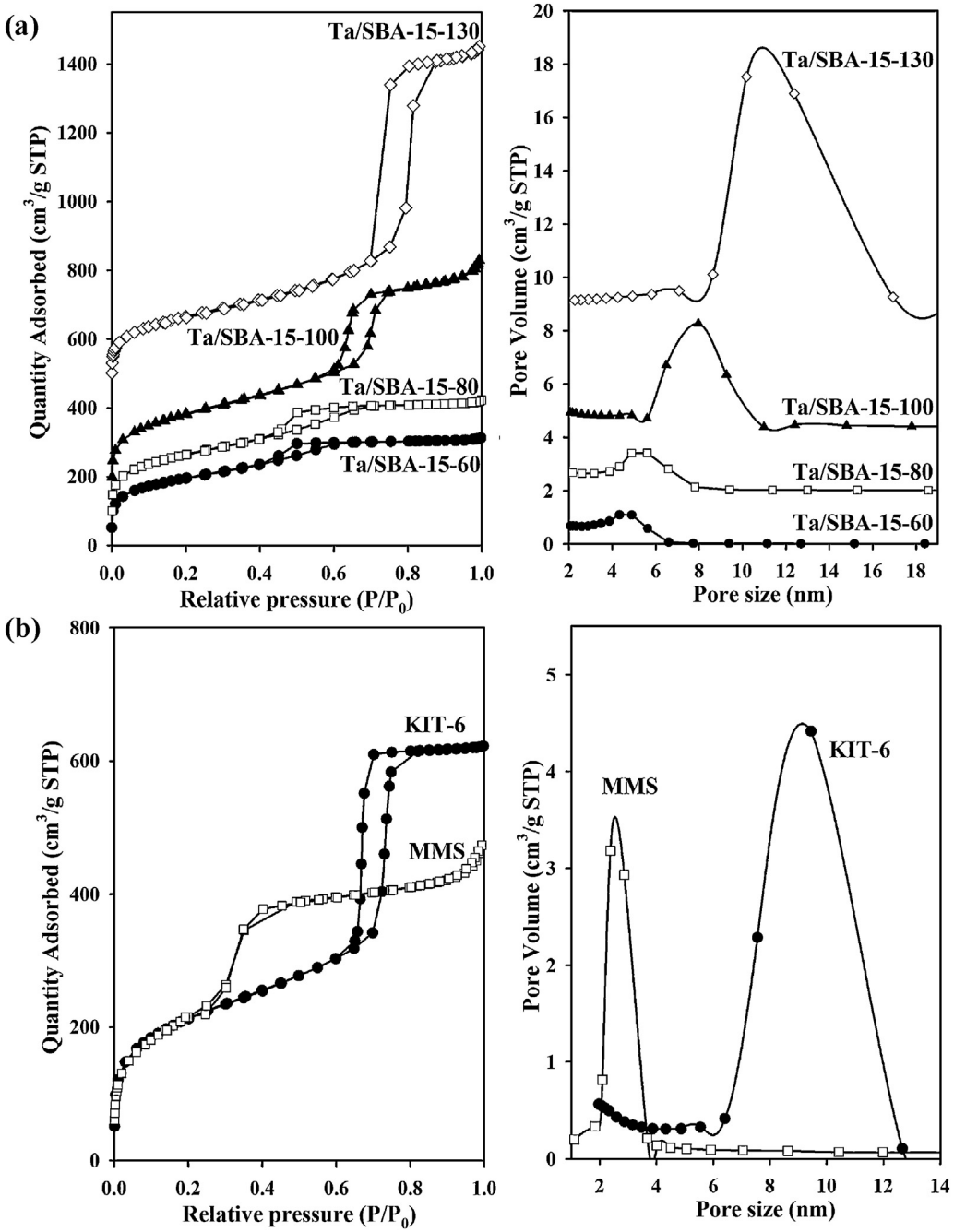


**Fig. 3.** Nitrogen sorption isotherms and pore size distributions of (a) Ta/SBA-15 supports with different hydrothermal temperature, and (b) Ta/KIT-6 and Ta/MMS supports. The isotherms for Ta/SBA-15-80, Ta/SBA-15-100, and Ta/SBA-15-130 are offset vertically by 50, 150, and 475 $cm^3$/g STP, respectively, and the pore size distributions for Ta/SBA-15-80, Ta/SBA-15-100, and Ta/SBA-15-130 are offset vertically by 2, 4.3, and 9 $cm^3$/g STP, respectively.

the results of the wide angle XRD patterns. From the above analyses, Ta species were highly dispersed on the silica supports. It might imply that the surface active Ta species mainly exist as an isolated $TaO_4$ species at low Ta content according to previous report [25].

### 3.2. Catalytic test for 1,3-butadiene production from ethanol and acetaldehyde

Fig. 7 shows the total conversion of ethanol (EtOH) and acetaldehyde (AA) and the BD selectivity of conventional silica-supported tantalum oxide catalysts (Ta/Aldrich and Ta/Merck) as well as tantalum oxide catalysts impregnated over various OMS supports with different mesostructures. Most of the Ta/OMS catalysts show superior reactants conversion and BD selectivity to those properties of the two commercial silica supported tantalum oxide catalysts. In addition, Table 2 shows that the formation of unidentified compounds, including mainly heavy compounds, was obviously reduced in the Ta/OMS catalysts compared to the conventional silica-supported tantalum oxide catalysts. This relatively good conversion and BD selectivity of Ta/OMS catalysts can be explained by the high surface area, which gives the good dispersion of active sites (tantalum oxide), and unique structural properties of the ordered mesoporous silica materials, such as their well-developed mesopore ordering and narrow mesopore size distribution, as discussed in Section 3.1.

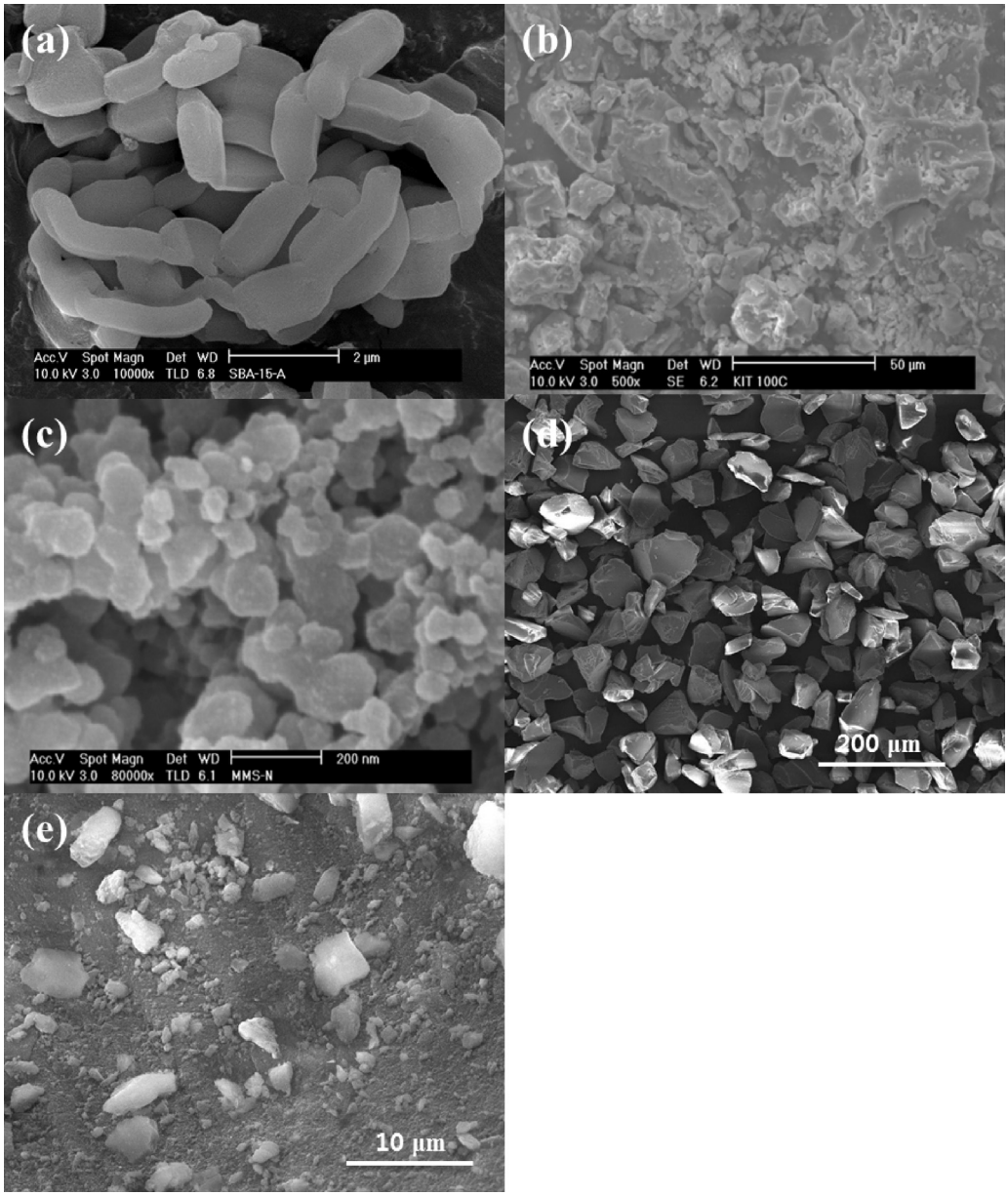


**Fig. 4.** SEM images of (a) Ta/SBA-15-100, (b) Ta/KIT-6, (c) Ta/MMS, (d) Ta/Merck, and (e) Ta/Aldrich catalysts.

As mentioned in Section 3.1, Ta/SBA-15-100 and Ta/KIT-6 have different pore structures, with a 2-D hexagonal (Ta/SBA-15-100) and a 3-D cubic (Ta/KIT-6) mesostructure, while the other structural properties of the two catalysts are similar, such as the BET-specific surface area, total pore volume, and pore size distribution. Fig. 7 also reveals the catalytic performance during BD production with respect to the mesostructural difference between the 2-D hexagonal (Ta/SBA-15-100) and 3-D cubic (Ta/KIT-6)

**Table 2**
Catalytic performance of 2 wt% $Ta_2O_5$ supported OMS and commercial silica catalysts in 1,3-BD production at 350 °C, LHSV of 1 $h^{-1}$ at 10 h.

| Sample | EtOH/AA conv. (%) | Carbon selectivity (C mol%) | | | | | | | | |
|---|---|---|---|---|---|---|---|---|---|---|
| | | Ethylene | Propylene | Butene isomers | 1,3-BD | Ethoxy ethane | Ethyl acetate | Crotonaldehyde | Acetic acid | Others[a] |
| Ta/SBA-15-60 | 31.4 | 8.7 | 1.9 | 1.5 | 72.8 | 6.4 | 1.8 | 0.6 | 0.4 | 6.0 |
| Ta/SBA-15-80 | 36.9 | 7.5 | 1.9 | 1.6 | 76.5 | 5.1 | 1.7 | 0.5 | 0.4 | 4.8 |
| Ta/SBA-15-100 | 46.9 | 4.5 | 1.8 | 2.0 | 79.8 | 4.0 | 1.1 | 1.0 | 0.2 | 5.8 |
| Ta/SBA-15-130 | 47.1 | 4.5 | 1.7 | 1.7 | 79.0 | 3.6 | 1.1 | 1.1 | 0.2 | 7.0 |
| Ta/KIT-6 | 38.2 | 3.2 | 1.5 | 2.0 | 78.5 | 3.2 | 1.2 | 1.0 | 0.2 | 9.3 |
| Ta/MMS | 40.7 | 4.3 | 1.8 | 1.8 | 77.9 | 3.5 | 1.3 | 0.8 | 0.2 | 8.4 |
| Ta/Aldrich | 30.8 | 1.4 | 1.0 | 1.0 | 72.4 | 1.6 | 1.4 | 0.5 | 0.8 | 19.9 |
| Ta/Merck | 32.5 | 2.4 | 1.6 | 1.0 | 74.6 | 2.5 | 1.6 | 0.6 | 0.3 | 15.5 |

[a] Unidentified compounds mainly consisting of heavier compounds than acetic acid in GC chromatography.

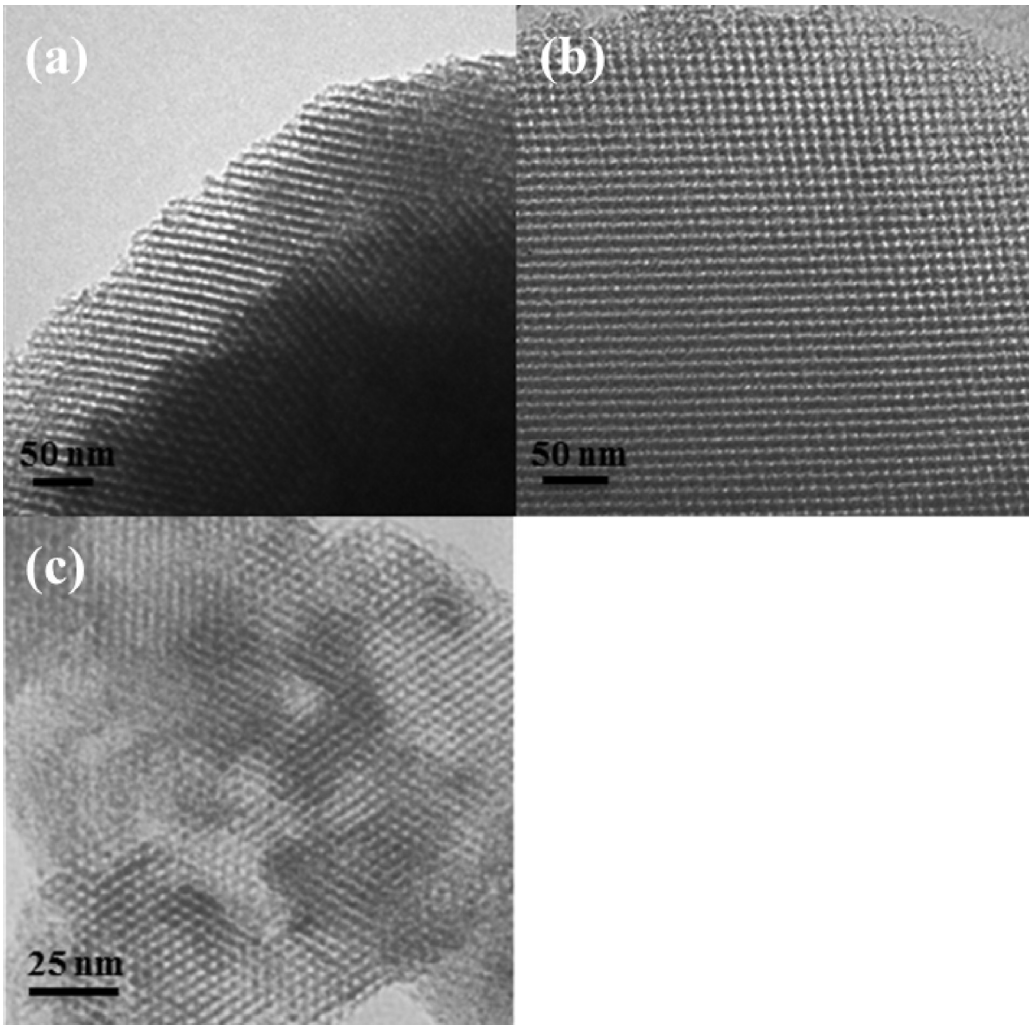


**Fig. 5.** TEM images of (a) Ta/SBA-15-100, (b) Ta/KIT-6, and (c) Ta/MMS OMS catalysts.

mesostructures. The conversion of EtOH/AA is slightly better for Ta/SBA-15-100 than for Ta/KIT-6; however, the BD selectivity is quite similar for both catalysts. This clearly indicates that the effect of the difference in OMS mesostructure like the SBA-15 and KIT-6 samples having a 2-D hexagonal and 3-D cubic pore ordering, respectively, is not critical on the optimization of Ta/OMS type catalysts for BD production from ethanol.

To investigate the effects of the mesopore size and to determine the optimum mesopore size, MMS and SBA-15 supported tantalum oxide catalysts with the same 2-D hexagonal mesostructure and five different mesopore sizes ranging from 2.5 to 10.9 nm were used for BD production from an EtOH/AA mixture. Fig. 8 shows the conversion and BD selectivity results of the Ta/MMS and Ta/SBA-15 catalysts with different pore sizes. Among the series of Ta/SBA-15 catalysts, the total conversion of EtOH and AA increases with an increase in the pore size of the Ta/SBA-15 catalysts up to 8.0 nm (Ta/SBA-15-100). The initial BD selectivity was also increased with an increase in the pore size of the Ta/SBA-15 catalyst, but the BD selectivity gap between the catalysts was gradually decreased as time elapsed. In the case of the Ta/SBA-15-130 catalyst with the largest mesopore size of 10.9 nm, the total conversion of the reactants and the BD selectivity were 47% and 79%, respectively, values which are quite similar to those of Ta/SBA-15-100. As the hydrothermal temperature increased from 100 to 130 °C, the mesopore size of the Ta/SBA-15 catalyst also increased, from 8.0 to 10.8 nm, whereas the BET-specific surface area dramatically decreased from 800 to 580 $m^2/g$ (Table 1). This implies that the reduction of the surface area of Ta/SBA-15-130 with a larger mesopore size produces catalytic results similar to those of Ta/SBA-15-100 with a smaller mesopore size. From the above results in the Ta/SBA-15 catalysts, a catalyst with both a large mesopore size and a high surface area would be a good candidate due to the good accessibility of the reactants and products and the high tantalum oxide dispersion.

As also shown in Fig. 8, interestingly, the Ta/MMS catalyst with the smallest mesopore size (pore size = 2.5 nm) shows catalytic performance similar to that of Ta/SBA-15-100 (pore size = 8.0 nm) despite the fact that the BET-specific surface area of Ta/MMS (790 $m^2/g$) is also similar to that of the Ta/SBA-15-100 catalyst (800 $m^2/g$). However, the size of the primary particle of the Ta/MMS catalyst is around thirty times smaller than that of the Ta/SBA-15-100 catalyst, as shown in Fig. 4. This indicates that the Ta/MMS catalyst has good catalytic performance due to its nano-sized particle morphology which induces its high external surface area. The high external surface area induced by the nano-sized morphology of Ta/MMS should facilitate the diffusion of reactants and products during the catalytic reaction, which is an effect similar to that of a larger mesopore size.

Based upon the results in Fig. 8, control of the pore size in same OMS, in this case the SBA-15 series, and the crystal size of OMS such as MMS, are very important for the optimization of the activity and for good selectivity during the ETB reaction, although OMS supports offer excellent potential support for the

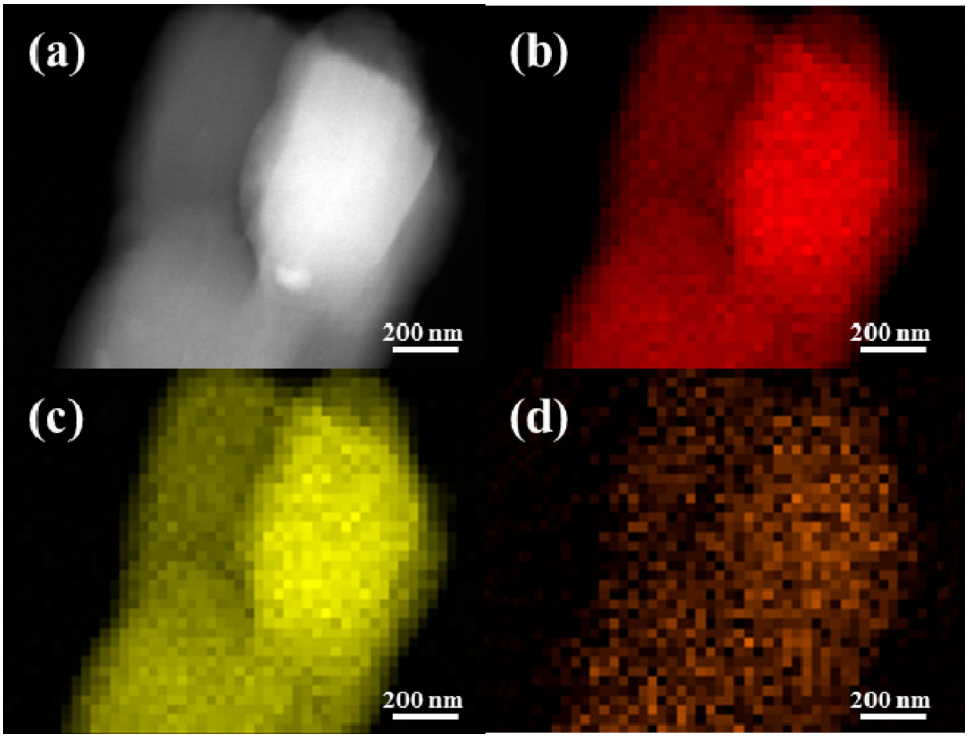


**Fig. 6.** (a) STEM image of Ta/SBA-15-100 sample. EDS mapping based on the peaks of (b) Si-Kα, (c) Ta-M, and (d) Ta-Lα.

ETB reaction. Considering that the main cause of catalytic deactivation in the ETB reaction is coking, the effect of the pore size and the crystal size of OMS supports can be reasonably explained by the good accessibility of the reactants and the products and the low formation of heavy compounds, which are often a source of coke.

Based upon the reaction results above, the BD productivity for Ta/SBA-15-100 catalyst is 0.35–0.4 ml of BD/ml of catalyst/h in LHSV of 1.0/h, which is much superior to Ta/Merck catalyst (0.22–0.24 ml of BD/ml of catalysts/h in LHSV of 1.0/h) and the literature catalyst (0.07–0.1 ml of BD/ml of catalysts/h in LHSV of 0.4–0.6/h, [10,12]). In other words, Ta/SBA-15-100 catalyst could have around 2–5 times the higher catalytic ability in BD productivity than conventional silica based catalyst or literature catalyst.

Finally, to verify the relatively superior availability in this ETB reaction of Ta/OMS catalysts, the catalytic durability by coking and regeneration ability of the ETB catalysts was also compared as shown in Fig. 9, which shows the longevity and regeneration results of Ta/SBA-15-100 and Ta/Merck catalysts. As clearly revealed in Fig. 9, Ta/SBA-15-100 catalyst developed in this work has superior catalyst life and regeneration ability to conventional silica based catalyst. In other words, besides initial BD selectivity and conversion, the long-term stability of catalytic performance of Ta/SBA-15-100 was also superior to that of Ta/Merck. In particular, the gap of BD selectivity between both catalysts was gradually increased with reaction time. Moreover, after regeneration, BD selectivity of Ta/Merck was not completely restored. From this result, it can be predicted easily that Ta/OMS catalysts will expand

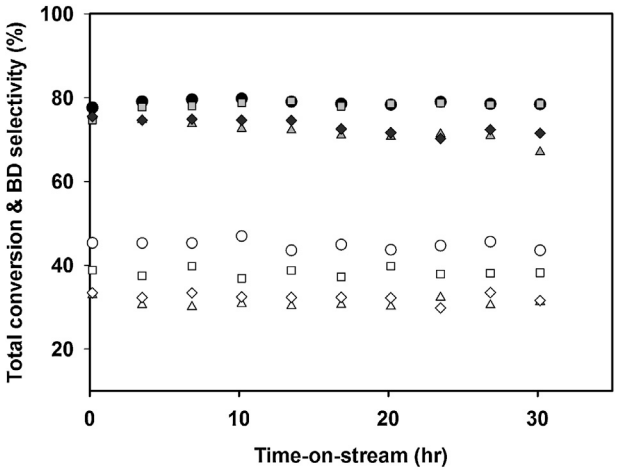


**Fig. 7.** EtOH/AA total conversion (open symbol) and BD selectivity (closed symbol) of various silica supported tantalum oxide catalysts (circle: Ta/SBA-15-100, square: Ta/KIT-6, triangle: Ta/Aldrich, diamond: Ta/Merck).

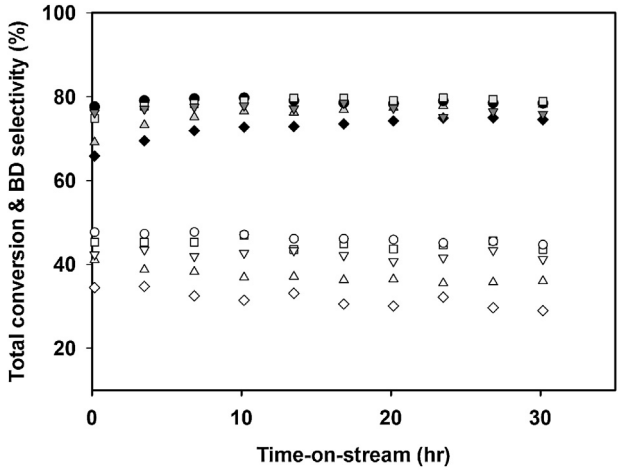


**Fig. 8.** EtOH/AA total conversion (open symbol) and BD selectivity (closed symbol) of various Ta/OMS catalysts (circle: Ta/SBA-15-130, square: Ta/SBA-15-100, triangle: Ta/SBA-15-80, diamond: Ta/SBA-15-60, down triangle: Ta/MMS).

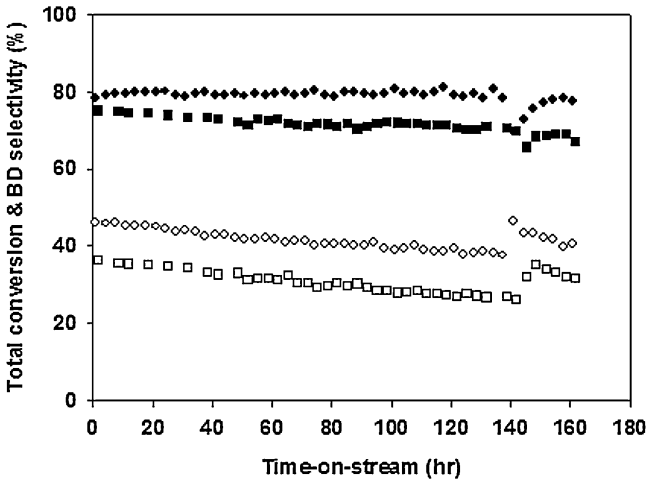


**Fig. 9.** EtOH/AA total conversion (open symbol) and BD selectivity (closed symbol) of Ta/SBA-15-100 (diamond) and Ta/Merck (square) catalysts for the comparison of catalyst longevity and regeneration ability: the regenerations were done at 500 °C for 5 h with air flow of 10 ml/min after reaction of 143 h.

regeneration period and this will greatly enhance process efficiency, compared to conventional silica based catalyst.

The amounts of coke formation for both spent Ta/SBA-100 and Ta/Merck catalysts after 40 h reaction was also observed by CHN elemental and TGA analysis (Table S1 and Fig. S1 in E-component). The weight losses of TGA analysis at the temperature range from 250 to 600 °C, which is temperature range for decoking, were 24.9 wt% and 17.3 wt% for Ta/SBA-100 and Ta/Merck, respectively. From theses CHN elemental analysis and TGA results, the amount of coke formation for Ta/SBA-100 catalyst is higher than to that of Ta/Merck catalyst. It could be due to the higher accumulated conversion on Ta/SBA-100 catalyst for the same reaction time. These results show that although Ta/OMS catalysts, especially Ta/SBA-100 having large pore size, have higher amount of coking source materials, they have high performance and longevity due to their less sensitivity to coking, compared to conventional silica Ta catalyst. In addition, according to Jones et al. [2], it has been reported that deactivation and 1,3-BD selectivity of ETB catalysts are related to pore blocking or obstruction by reactants and products. Therefore it should be related to the pore size of catalysts and larger pore materials show better catalytic performance than smaller pore material due to the less sensitivity of large pores to deactivation by coking. From the literature and the CHN elemental analysis and TGA results of two catalysts, it could be concluded that as a catalyst for ETB reaction, Ta/SBA-15-100 having uniform mesopores and large-pore size would show higher catalytic longevity by its less sensitivity to coking as well as catalytic activity than Ta/Merck catalyst having non-uniform pores and small-pore size.

## 4. Conclusion

In this study, we successively synthesized various OMS supports (SBA-15 series, KIT-6, MMS) to determine the potential of OMSs as a catalytic support in the ETB reaction compared to conventional silica supports. Moreover, we specified the effect of the mesopore structure, pore size and crystal size of the OMS supports. These findings are outlined below.

Ta/OMS catalysts would show better coke tolerance and catalytic longevity as well as catalytic activity than conventional silica based catalysts. In particular, Ta/SBA-15-100 catalyst could have around 2–5 times the higher catalytic ability in BD productivity than conventional catalysts.

From comparison of SBA-15-100 (2-D) and KIT-6 (3-D) it was found that the ETB reaction performance levels, especially the BD selectivity, of tantalum oxide catalysts were not very different from with regard to the type of OMS with a different pore structure.

However, it can be suggested that the pore size in the same type of OMS, especially regarding the SBA-15 series, has a great influence on the activity and selectivity of tantalum oxide catalysts in the ETB reaction. Thus, we could determine that the pore size of SBA-15-100 is optimum for the ETB catalyst.

In addition, the Ta/MMS catalyst shows ETB performance similar to that of Ta/SBA-15-100 despite the fact that MMS has the smallest pore size among the OMS supports synthesized in this study. Hence, the crystal size of OMS is very important when seeking to optimize the catalytic performance in the ETB reaction.

Finally, these effects of the pore size and the crystal size of OMS supports could be reasonably explained by the good accessibility of the reactants and products and the good coke tolerance of the catalysts. In conclusion, in this study, Ta/OMS catalysts, especially Ta/SBA-15-100, could be developed as high potential ETB catalysts to overcome the demerit of conventional silica based catalysts and to greatly improve this process efficiency.

## Acknowledgments

The authors would like to acknowledge the funding from KRICT's own project program.

## Appendix A. Supplementary data

Supplementary data associated with this article can be found, in the online version, at http://dx.doi.org/10.1016/j.apcatb.2013.12.023.

## References

[1] E.V. Makshina, W. Janssens, B.F. Sels, P.A. Jacobs, Catal. Today 198 (2012) 338–344.
[2] M.D. Jones, C.G. Keir, C.D. Iulio, R.A.M. Robertson, C.V. Williams, D.C. Apperley, Catal. Sci. Technol. 1 (2011) 267–272.
[3] S.K. Bhattacharyya, N.D. Ganguly, J. Appl. Chem. 12 (1962) 105–110.
[4] S.K. Bhattacharyya, B.N. Avasthi, Ind. Eng. Chem. Process Des. Dev. 2 (1963) 45–51.
[5] S.K. Bhattacharyya, S.K. Sanyal, J. Catal. 7 (1967) 152–158.
[6] B.B. Corson, H.E. Jones, C.E. Welling, J.A. Hinckley, E.E. Stahly, Ind. Eng. Chem. 42 (1950) 359–373.
[7] H. Niiyama, S. Morii, E. Echigoya, Bull. Chem. Soc. Jpn. 45 (1972) 655–659.
[8] R. Ohnishi, T. Akimoto, K. Tanabe, J. Chem. Soc., Chem. Commun. (1985) 1613–1614.
[9] S. Kvisle, A. Aguero, R.P.A. Sneeden, Appl. Catal. 43 (1988) 117–131.
[10] W.J. Toussaint, J.T. Dunn, D.R. Jackson, Ind. Eng. Chem. 39 (1947) 120–125.
[11] W.M. Quattlebaum, W.J. Toussaint, J.T. Dunn, J. Am. Chem. Soc. 69 (1947) 593–599.
[12] E.E. Stahly, H.E. Jones, B.B. Corson, Ind. Eng. Chem. 40 (1948) 2301–2303.
[13] H.E. Jones, E.E. Stahly, B.B. Corson, J. Am. Chem. Soc. 71 (1949) 1822–1828.
[14] B.B. Corson, E.E. Stahly, H.E. Jones, H.D. Bishop, Ind. Eng. Chem. 41 (1949) 1012–1017.
[15] P.M. Kampmeyer, E.E. Stahly, Ind. Eng. Chem. 41 (1949) 550–555.
[16] S.K. Bhattacharyya, B.N. Avasthi, J. Appl. Chem. 16 (1966) 239–244.
[17] V.V. Ordomskiy, V.L. Sushkevich, I.I. Ivanova, WO/2012/015340 (2012).
[18] M. Choi, W. Heo, F. Kleitz, R. Ryoo, Chem. Commun. (2003) 1340–1341.
[19] T.-W. Kim, F. Kleitz, B. Paul, R. Ryoo, J. Am. Chem. Soc. 127 (2005) 7601–7610.
[20] H.S. Jeong, S.Y. Jeong, J.M. Lee, D.J. Yim, S.K. Ryu, J. Ind. Eng. Chem. 5 (1999) 247–252.
[21] M. Kruk, M. Jaroniec, K.P. Gadkaree, J. Colloid Interface Sci. 192 (1997) 250–256.
[22] C.P. Jaroniec, M. Kruk, M. Jaroniec, A. Sayari, J. Phys. Chem. B 102 (1998) 5503–5510.
[23] M. Jaroniec, M. Kruk, J.P. Olivier, Langmuir 15 (1999) 5410–5413.
[24] T. Ushikubo, K. Wada, Appl. Catal. A: Gen. 124 (1995) 19–31.
[25] Y. Chen, J.L.G. Fierro, T. Tanaka, I.E. Wachs, J. Phys. Chem. B 107 (2003) 5243–5250.